
Data report: core-log-seismic integration and time-depth relationships at IODP Expedition 341 Southern Alaska Margin Sites U1420 and U1421, Bering Trough, Gulf of Alaska¹

Wesley A. Clary,² Lindsay L. Worthington,² Angela L. Slagle,³ and Hugh Daigle⁴

Chapter contents

Abstract	1
Introduction	1
Methods and materials	2
Results	5
Acknowledgments	6
References	6
Figures	8
Tables	25

Abstract

We present a time-depth relationship for Integrated Ocean Drilling Program (IODP) Expedition 341 Southern Alaska Margin Sites U1420 and U1421 using high-resolution multichannel seismic, core, and logging data. Calibrating and combining core and logging data at each site minimizes data gaps in physical properties information. Remaining data gaps were interpolated using spline fitting in order to provide continuous estimates of bulk density and compressional wave velocity for the full drilled interval. We use the interpolated physical property curves for bulk density and compressional wave velocity at each site to generate synthetic seismic traces. At Site U1421, vertical seismic profiling further constrained the time-depth relationship and was used to calibrate the velocity curve and provide input for the initial velocity model during the tie. Finally, we matched simulated reflectors in the synthetic trace with events in the nearby seismic traces and established a time-depth relationship at each site.

Introduction

A major goal of Integrated Ocean Drilling Program (IODP) Expedition 341 Southern Alaska Margin was investigation of interrelationships between tectonic processes, paleoclimate, and glacial activity. One of the primary expedition research questions focuses on if and how large-scale mass redistribution through rapid sedimentation or glacial advance and retreat can alter the geometry of tectonic wedges in a temperate glaciated margin (e.g., Berger et al., 2008; Worthington et al., 2010). High-resolution sequence stratigraphic and structural studies of the offshore sedimentary record are essential to establishing connections between tectonic deformation and glacial processes. Developing accurate chronological relationships requires careful calibration between seismic and well-derived data. Here, we focus on core-log-seismic integration of Sites U1420 and U1421 near the Bering Trough offshore southeast Alaska. Coring at these sites (Fig. F1) sampled sediments of the Pamplona fold and thrust belt, which has accommodated shortening during Yakutat microplate convergence with North America since ~25 Ma (Worthington et al., 2010).

¹Clary, W.A., Worthington, L.L., Slagle, A.L., and Daigle, H., 2017. Data report: core-log-seismic integration and time-depth relationships at IODP Expedition 341 Southern Alaska Margin Sites U1420 and U1421, Bering Trough, Gulf of Alaska. In Jaeger, J.M., Gulick, S.P.S., LeVay, L.J., and the Expedition 341 Scientists, *Proceedings of the Integrated Ocean Drilling Program, 341*: College Station, TX (Integrated Ocean Drilling Program). doi:10.2204/iodp.proc.341.204.2017

²Department of Earth and Planetary Sciences, University of New Mexico, 221 Yale Boulevard NE, Albuquerque NM 87131-0001, USA.

Correspondence author: wesclary@unm.edu

³Lamont-Doherty Earth Observatory, Columbia University, 212A Borehole, Palisades NY 10964-8000, USA.

⁴Department of Petroleum and Geosystems Engineering, University of Texas, 200 East Dean Keeton Street, Stop C0300, Austin TX 78712-1585, USA.



Constraining the rate, amount, and distribution, of sedimentation is important to evaluating regional hypotheses relating shelf development, tectonic activity, and paleoclimate variations. Well and logging data from Expedition 341 provides important stratigraphic, physical property, and age data recorded in depth which facilitates development of a constrained stratigraphic model that can be extended across the shelf if carefully integrated with local and regional seismic surveys. The challenging drilling environment resulted in limited core recovery due to large clasts and poorly consolidated material and difficult logging mostly due to borehole instability (see the “[Site U1420](#)” and “[Site U1421](#)” chapters [Jaeger et al., 2014b, 2014c]). These factors result in significant data gaps that present challenges with core-log-seismic integration. We attempt to bridge data gaps by using aggressively fitted splines in constrained intervals where data coverage did not include significant gaps greater than ~25 m. In poorly constrained intervals, with gaps as large as ~270 m, we apply spline fits with a higher smoothness parameter (Silverman, 1985). The smoother splines typically fit the data less well in constrained intervals but result in more conservative estimates of variability where measurements are lacking. We used the continuous spline curves to generate synthetic seismograms at the site and matched the synthetic traces with high-resolution seismic survey EW0408 Lines GOA 2503 and GOA 2505 according to traditional well-tie techniques (e.g., White, 1997; White and Simm, 2003). We used these time series and depth series matches to develop the final time-depth relationship (TDR) presented here that can be used to improve the calibration of developing age models. This study advances Expedition 341 scientific goals by providing a core-, log-, and seismic-constrained TDR for two sites on the southern Alaska shelf.

Methods and materials

Physical property data

Expedition 341 collected core and logging data on the continental shelf and slope at Sites U1420 and U1421 (Fig. [F1](#)). During drilling, the shipboard science party performed measurements of various physical properties at multiple scales and resolutions. After the core came on deck, the whole-round core passed through the Special Task Multisensor Logger (STMSL) where gamma ray attenuation (GRA) bulk density and magnetic susceptibility measurements were collected. After a period of temperature equilibration, the core was passed through the Whole-Round Multisensor Logger (WRMSL), which recorded GRA bulk density, magnetic susceptibility,

and compressional wave velocity (using the *P*-wave velocity logger [PWL]). Natural gamma ray (NGR) measurements were taken before the splitting the cores into working and archive halves. The archive half then passed through the Section Half Multisensor Logger (SHMSL) where reflection spectroscopy, colorimetry, magnetic susceptibility, and laser split-core surface analyses were performed. From the working halves, point measurements of compressional wave velocity were taken with the *P*-wave caliper (PWC) instrument and discrete samples were collected for moisture and density (MAD) measurements, which consisted of bulk density, water content, porosity, and grain density. This process is described in detail in the “[Methods](#)” chapter (Jaeger et al., 2014a) and is schematically illustrated in Figure [F2](#). Core recovery was hindered at both sites by large clasts that jammed recovery equipment and resulted in 139.91m of recovered core (14%) over the 1020.8 m interval at Site U1420 (see the “[Site U1420](#)” chapter [Jaeger et al., 2014b]). At Site U1421, three holes were drilled, with Hole U1421A reaching total penetration of 1432.4 mbsf (driller’s seafloor depth = 729.7 m), and total recovery from all holes at Site U1421 was ~176 m.

At Sites U1420 and U1421, shipboard scientists deployed a wireline tool string, which included NGR, sonic velocity, and resistivity tools (see the “[Site U1420](#)” and “[Site U1421](#)” chapters [Jaeger et al., 2014b, 2014c]). As a result of concerns about borehole stability during logging, the density tool with its radioactive source was not included in this tool string; thus, no in situ density measurements were made at Sites U1420 and U1421. The logged interval, excluding the bottom-hole assembly (BHA), at Site U1420 was 89–288 m wireline log matched depth below seafloor (WMSF) due to borehole instability (see the “[Site U1420](#)” chapter [Jaeger et al., 2014b]). At Site U1421, the logged interval was below the BHA at 92 m WMSF and extended to 695 m WMSF. At Site U1421, we used vertical seismic profile (VSP) constraints from six stations in the borehole to constrain the TDR between 1.278–1.641 s two-way traveltime (TWT) and 284.7–687 m WMSF (Table [T1](#)).

More details about core handling, logging data collection, and processing methods as well as tool string and instrument technical data can be found in the “[Methods](#)” chapter (Jaeger et al., 2014a). Table [T2](#) summarizes site data including location and physical properties measurement availability by source. Logging summaries and plots are shown in Figure [F3](#). Depth scales and datums are described in “[Stratigraphic correlation](#)” in the “[Methods](#)” chapter (Jaeger et al., 2014a). We approached the well tie process based on the methods of White and Simm (2003) in

a few steps, including the development of initial velocity models, synthetic seismic generation, wavelet extraction, generation of a new synthetic seismic trace, and finally, conservative visual seismic-to-synthetic matching.

Data conditioning and compilation

In general our strategy was to favor a log-centric approach to the data conditioning for two reasons: (1) the core data seemed to be noisy and had more outliers in comparison to the logging data and (2) we expect the in situ logged values to be more consistent with conditions reflected in the seismic data than measurements derived post situ. Core-based and in situ logging data may be different for a number of reasons, such as sampling rate, measurement depth of investigation, datum mismatch, borehole and core irregularity, and coring practices (e.g., see the “[Methods](#)” chapter [Jaeger et al., 2014a] and [Daigle and Piña, 2016](#)). For the purposes of this study, we applied minimal or no specific corrections for such factors in preparing the data compilations. Shipboard core-based measurements were collected in a variety of methods including track-based sensors, which measure properties of the whole or split-core; by analysis of discrete volumetric samples; and by using point-based instruments. Instrument response functions, the effects of core recovery technique (advanced piston coring [APC], extended core barrel [XCB], etc.), and a volumetric-based correction are discussed in Walczak et al. (2015). At Sites U1418 and U1417, the correction applied by Walczak et al. (2015) corrected for sediment compaction, variable recovered core diameter, and changes in the gas content of the sediment column but reduced the variance of NGR and bulk density measurements by ~20% and 50%, respectively, and after correction the largest changes in GRA bulk density were correlated with changes in coring technique. In order to preserve variability in the final synthetic seismic traces, our compilation treated all core-based data with equal weight and without adjustment for instrument effects or core recovery technique.

Site U1420 density and velocity compilation

At Site U1420, the bulk density data we included in the compilation were derived from WRMSL measurements where outliers ($<1 \text{ g/cm}^3$) were removed from the data set and then smoothed by a 19-sample moving average; typically this resulted in a moving window of 45 cm. STMSL bulk density data were not available at this site, but these measurements were at a lower spatial resolution than WRMSL GRA bulk density measurements, used similar sensors, were

not given time for temperature equilibration, and were generally used for guiding drilling operations during the expedition (see the “[Methods](#)” chapter [Jaeger et al., 2014a]). Velocity data consisted of a logged interval with the Dipole Shear Sonic Imager (DSI) and PWC core measurements. We cleaned the PWC data of outlier measurements $<1.5 \text{ km/s}$. We compiled log data on the WMSF depth scale, which is based on matching a spike in the gamma ray log with the seafloor. Core data were compiled on the core depth below seafloor, Method A (CSF-A), depth scale, which is an initial scale based on the advancement of the drill string during coring (see “[Stratigraphic correlation](#)” in the “[Methods](#)” chapter [Jaeger et al., 2014a]). Core-based CSF-A and logging WMSF depth scales were used together directly, which may introduce error because of a number of drilling effects (see the “[Methods](#)” chapter [Jaeger et al., 2014a]), which we also discuss briefly here.

Site U1421 density and velocity compilation

At Site U1421, we compiled bulk density data from core for the STMSL, WRMSL sources, and from Holes U1421A–U1421C, which we cleaned of outliers beyond 2 standard deviations of the mean for each instrument source. Next, we culled any remaining measurements $<1 \text{ g/cm}^3$. Finally, we smoothed these compiled density data with a 19-sample moving average (45 cm) on the core composite depth below seafloor, Method B (CCSF-B), depth scale, which was developed by splicing Holes U1421A–U1421C accounting for ship heave and applying an affine value to adjust for postrecovery expansion (see “[Stratigraphic correlation](#)” in the “[Methods](#)” chapter [Jaeger et al., 2014a]). Compressional wave velocity data at Site U1421 included both core and logging data. We combined core-based velocity measurements from the PWL, WRMSL, and PWC on the CCSF-B depth scale. The sonic log was used on the WMSF depth scale, and after removal of outliers beyond 3 standard deviations from the moving 40 m average, we combined it with the core-based measurements, which were shifted so that their mean was equal to the mean value from logging data in the overlapping interval. This shift to the core measurements, an increase of 53 m/s, served as a simple method to calibrate the wireline-logged and core-derived measurements in such a way to approximate in situ logged measurements (Fig. F4).

Data fitting

In Matlab R2015a software, we fit the cleaned and processed data described above by spline approximations of various smoothness. We employed a strategy

of aggressively fitting the data in constrained intervals, which tended to create artificial data variability and introduce unrealistic predictions, such as bulk density <1 g/cm³, or negative velocity estimates in unconstrained intervals. To overcome these artifacts of overfitting in large poorly constrained gaps and often also where the only source was core-based data, smoother splines were used for interpolation. To create data sets comparable to those generated in the logging operations and create continuous physical property records for the full drilled interval, we resampled the compiled smoothed data at 0.1524 m spacing, consistent with the logging rate. The final interpolated curves, goodness of fit characteristics, and original measurements are shown in Figures F5, F6, F7, F8, and F9 and discussed in Results.

Initial velocity models

At Site U1420, the initial velocity model was constructed directly from the compiled velocity curve, which included both logging and core data. We created initial interval velocity models for each site using the continuous velocity curves. The primary role of calibration at this site, as seen in Figure F10A, is to initially match the seafloor between the velocity curve, the seismic line (259 m WMSF and 330 ms TWT, respectively), and the interval velocity model at a 5 m sample spacing. At Site U1421, we used results from the VSP experiment to create an initial velocity structure against which to calibrate the velocity curve (Fig. F10B). We used the measured depth of the seafloor and the TWT of the positive seafloor arrival (729.7 m WMSF and 980 ms, respectively) in the seismic line with the time-depth matches of the check shots (Table T3) to create the initial seven-layer velocity model. In Petrel 2015 software, we performed calibration of the velocity curve to the VSP by addition of a linearly interpolated drift value between check shots as well as the interval velocity calculations.

Synthetic seismic generation

At each site, we iteratively generated a synthetic seismic trace; an initial convolution with calculated well reflectivity series and a Ricker wavelet provided a rough initial calibration. Next, any necessary bulk shift was applied to obtain a depth match between the seafloor in the drilling and seismic data. We used the Roy White wavelet extraction method at each site in Petrel 2015 to estimate source wavelet information using the continuous physical property curves and trace recordings near the hole. This method refines the tie by using cross-correlation of

the hole reflectivity and seismic trace amplitudes to extract a deterministic wavelet (White, 1980). The algorithm produces a wavelet by using the ratio of cross-correlation of the reflectivity and seismic trace in the frequency domain (by fast Fourier transform) to the autocorrelation of reflectivity plus white noise. Spectral properties of wavelets used in this analysis are summarized in Figure F11. We convolved these deterministically extracted wavelets with the reflectivity series to create the synthetic seismic traces used in the synthetic-to-seismic matching process.

At Site U1420, we generated the synthetic seismic at the hole location first by convolution with the Ricker wavelet in Figure F11 (128 ms length and central positive peak at zero), and then any necessary bulk shift was applied to assure that the data aligned such that the seafloor time-depth match occurred near the positive seafloor reflection. Next, we performed convolution with a deterministically extracted wavelet (Fig. F11) according to the White method (White, 1980). Figure F12 shows the synthetic trace in the hole, nearby seismic traces from Line GOA 2505, interval velocity, and calculated reflection coefficients in both TWT and meters below sea level on the seismic depth scale (SSL). At Site U1421, we generated the synthetic seismic trace illustrated in Figure F13 using the deterministically extracted wavelet at this location after convolution with the same Ricker wavelet, as previously described, and bulk shift to maintain alignment of the top of the log with the positive reflection of the seafloor.

Seismic-to-synthetic matching

The traditional well tie method correlates the seismic recording and the synthetic seismic trace at the hole location (White, 1997). We made matches by visually identifying key horizons in the synthetic seismic trace generated in each hole and events in the survey near the hole location. In order to finally calibrate the hole and seismic, it is common practice to execute these matches by small adjustments to the velocity model in order to increase the correlation between the synthetic trace and the seismic data (White and Simm, 2003). In this way the velocity model, and thus the TDR, depends initially on the velocity log, or velocity log and check shots in the case of Hole U1421A, and the final velocity model is determined by the applied adjustments from the visual matches (e.g., White and Simm, 2003). We applied the calibration procedure described above as the basis for the development of a TDR at each site (Tables T1, T4).

Results

Site U1420

In Matlab R2015a we fitted four splines to the bulk density data for Site U1420, and based on the size of the data gap the splines were selectively sampled to create a continuous, partially interpolated record consistent with the sampling rate of typical logging (Fig. F3). We fit the upper ~170 m with a spline achieving $R^2 = 0.800$ and root mean squared error (rmse) = 0.0746 with the moving average of the data compilation in this region (Fig. F4). The data gap between ~170 and 450 m CSF-A was interpolated with a minimum curvature spline, which was nearly equivalent to a linear fit between samples on either side of the gap. We fit the lower interval with an aggressive spline, which reached $R^2 = 0.8032$ and rmse = 0.0449 deeper than ~450 m CSF-A. For gaps near 500–550 and 700–750 m CSF-A, we interpolated with a smoother spline with a lower $R^2 = 0.38$ and rmse = 0.0842 compared to the data compilation. This selective sampling strategy resulted in conservative estimates of variability in poorly constrained intervals.

We created the continuous *P*-wave velocity curve from a compilation of logged and core-derived measurements where CSF-A and WMSF depth scales were used together directly. This may introduce error because in the CSF-A scale drilling effects such as core expansion caused by overburden release, compression during coring, and coring method are not compensated; these effects are typically on the order of 10%–20% (see “Stratigraphic correlation” in the “Methods” chapter [Jaeger et al., 2014a]). In sum, these sampling biases are difficult to accurately quantify and often affect a difference between core- and log-derived measurements. The velocity curve presented here below the logged interval (i.e., deeper than 288 m WMSF) likely represents minimum estimates because the apparent average velocity decreases with depth as opposed to a typical compaction trend and also because these measurements were collected on the WRMSL, which tends to be negatively affected by incompletely full core liners (Walczak et al., 2015). These measurements were fitted with one of three splines depending on the availability of data in the depth interval (Fig. F5). In the upper 270 m, we sampled from a spline achieving $R^2 = 0.9287$ and rmse = 0.0454 compared to the full data compilation. Deeper than 270 m on the combined CSF-A/WMSF scale, we fit the data using two splines. The more aggressive fit had $R^2 = 0.7774$ and rmse = 0.1020. Except for data gaps near 270–550 and 700–780 m on the combined depth scale, where the aggressive fit predicts unusually large variability, we sample from this spline. The spline that we used

for interpolation in the poorly constrained intervals reached $R^2 = 0.6698$ and rmse = 0.1165 with data from the compilation deeper than ~270 m on the combined depth scale.

Figure F14 summarizes the cross-correlation before and after the tie. The cross-correlation is a statistic commonly used to quantify the similarity of signals based on a lag time or offset. In this case we desire a maximum cross-correlation value between our synthetic and seismic signals near zero lag time close to the site. Before visual matching, the maximum cross-correlation within five traces of the site, nearest Trace 2622 on Line GOA 2505, was 0.367 with Trace 2619 with a lag of 13 ms in the 340–1410 ms window. At the site trace, the cross-correlation was calculated as –0.118 at 0 ms lag. After a bulk shift and visual matching, we calculate that the maximum cross-correlation occurred at Trace 2624 and 3 ms lag. At Trace 2622, the maximum cross-correlation was calculated to be 0.188 at 0 ms lag, whereas the maximum cross-correlation for this trace, 0.350, occurred with 3 ms lag. To avoid overinterpretation of the data, we made minimal matches and shifts ($n = 4$) to achieve visually acceptable results between the synthetic and seismic traces (Fig. F15). Although the correlation is low compared to sites with more complete drilling records (e.g., the well to seismic tie in White and Simm [2003] reported an R^2 of ~0.87) the overall character of the seismic and synthetic traces agrees well visually among their major trends and reflectors. High-amplitude reflectors in seismic Line GOA 2505 near 475 and 895 ms TWT are well matched by reflectors in the synthetic seismic at ~390 and 820 m seismic depth below sea level (SSL). Low core recovery, variable data quality and source, data compilation handling, and a short logged interval relative to the length of the well-to-seismic tie are likely responsible for the low correlation. Figure F15, shown with the final TDR (Table T4), better illustrates the quality of the tie.

The preliminary TDR created shipboard (see Fig. F11 in the “Site U1420” chapter [Jaeger et al., 2014b]) may represent a maximum depth relationship by using linear approximation through WRMSL velocity measurements near 680 and 900 m CSF-A. We observe that values here are notably higher than the mean of the WRMSL velocity measurements overall but are low compared to the expected in situ logging trend. Unlike a typical compaction trend that increases with depth, the apparent average velocity decreases with depth at this site. Only a single WRMSL density measurement above the logged interval was available, and this measurement value is low among the data set, which results in the calculation of a smaller than expected reflection coefficient

at the seafloor. We directly used bulk density values from the WRMSL, which are likely minimum values compared to ideal recovery with perfectly full core liners or an equivalently wireline logged section measured in situ (see the “Site U1420” chapter [Jaeger et al., 2014b]). Although this effect may be particularly important below the end of the logged interval (i.e., below 288 m WMSF), the variability of the core-derived measurements provides changes in the synthetic trace which we correlate to events in the seismic traces near the well location.

Site U1421

At Site U1421, we derived a bulk density compilation used for data fitting and interpolation from STMSL and WRMSL measurements from Holes U1421A–U1421C on the CCSF-B scale. We fitted two splines to the data and selectively sampled from them to create a continuous record. Using the more aggressive fit, we achieved $R^2 = 0.9309$ and $\text{rmse} = 0.0599$ with the compilation moving average for the full interval (Fig. F6). Although we found that it was possible to achieve higher R^2 values, the fit presented here is the best fit constrained such that no density $< 1 \text{ g/cm}^3$ was predicted. At ~150–220, near 410, and 500–575 m CCSF-B, we sampled a smoother spline fit with $R^2 = 0.6980$ and $\text{rmse} = 0.1404$.

The full velocity compilation used for spline fitting was created by compiling the logged measurements with the core compilation measurements. In the upper 92 m, we sampled the spline-fitted data from the core compilation with $R^2 = 0.7908$ and $\text{rmse} = 0.0674$. The bottom interval consisted of the fitted log-derived compilation from a spline with $R^2 = 0.9718$ and $\text{rmse} = 0.03833$. Although both log and core data were available for a short interval, in the area of overlap we sampled from the spline fitted to the wireline-logged data.

We made matches between the synthetic and seismic traces, which were minimal in number ($n = 14$) and scale. Before matching, the maximum cross-correlation within five traces of the site, nearest Trace 411 on Line GOA 2503, was 0.417 with Trace 414 at -1 ms lag when correlating the 980–1650 ms window. At the site trace we calculate the cross-correlation with the synthetic at 0 ms lag to be 0.365, which was also the maximum in the trace window at any lag. After matching, the maximum cross-correlation, 0.500, occurred at Trace 413 with 0 ms lag. At Trace 411, the nearest to the site, the zero-lag cross-correlation was 0.413 and the trace maximum cross-correlation, 0.448, occurred at 1 ms lag (Fig. F16). Again, despite the low correlation compared to ties based on more complete data, we find that the character of

the seismic and synthetic traces agrees well visually in overlay (Fig. F15). High-amplitude reflectors on seismic Line GOA 2503 near 1279, and 1620 ms TWT match well with the synthetic at 1020 and 1395 m SSL. The final TDR is shown in Table T1 with reference to both the SSL and meters seismic depth below seafloor (SSF) datums. Additionally, we note the high agreement between our final TDR and the check shot time-depth constraints, which suggests a well-calibrated model.

Application to previous work

We apply the TDR to estimate depths of several reflectors in seismic Lines GOA 2503 and GOA 2505. These sections and horizons are discussed and interpreted in Worthington et al. (2010) and the “Site U1420” and “Site U1421” chapters (Jaeger et al., 2014b, 2014c). Here, we simply provide a summary table of the depths of these horizons as calculated by our TDR (Fig. F17). At Site U1420, we were able to provide depth estimates for Horizons H1A, H1B, H1, H2A, H2B, H2C, H2D, and H2, which had TWTs less than ~1550 ms. At Site U1421 we provided depth estimates for Horizons H1B, H1, and H2A. For each location we estimated the TWT from the appropriate seismic section near the well and interpolated from our final TDR to generate depth estimates.

Acknowledgments

All data used in this report were collected aboard the R/V *JOIDES Resolution* during Integrated Ocean Drilling Program Expedition 341, June–August 2013. We thank the shipboard science party, captain, and crew for making this work possible and Dr. Gail Christeson for helpful discussion. This research was partially funded by a postexpedition award to L. Worthington and a UNM-EPS Murdoch Fellowship to W. Clary.

References

- Berger, A.L., Gulick, S.P.S., Spotila, J.A., Upton, P., Jaeger, J.M., Chapman, J.B., Worthington, L.A., Pavlis, T.L., Ridgway, K.D., Willems, B.A., and McAleer, R.J., 2008. Quaternary tectonic response to intensified glacial erosion in an orogenic wedge. *Nature Geoscience*, 1:793–799. <http://dx.doi.org/10.1038/ngeo334>
- Daigle, H., and Piña, O.L., 2016. Data report: permeability, consolidation properties, and grain size of sediments from Sites U1420 and U1421, offshore southern Alaska. In Jaeger, J.M., Gulick, S.P.S., LeVay, L.J., and the Expedition 341 Scientists, *Proceedings of the Integrated Ocean Drilling Program*, 341: College Station, TX (Integrated Ocean Drilling Program). <http://dx.doi.org/10.2204/iodp.proc.341.201.2016>

- Jaeger, J.M., Gulick, S.P.S., LeVay, L.J., Asahi, H., Bahlburg, H., Belanger, C.L., Berbel, G.B.B., Childress, L.B., Cowan, E.A., Drab, L., Forwick, M., Fukumura, A., Ge, S., Gupta, S.M., Kioka, A., Konno, S., März, C.E., Matsuzaki, K.M., McClymont, E.L., Mix, A.C., Moy, C.M., Müller, J., Nakamura, A., Ojima, T., Ridgway, K.D., Rodrigues Ribeiro, F., Romero, O.E., Slagle, A.L., Stoner, J.S., St-Onge, G., Suto, I., Walczak, M.H., and Worthington, L.L., 2014a. Methods. In Jaeger, J.M., Gulick, S.P.S., LeVay, L.J., and the Expedition 341 Scientists, *Proceedings of the Integrated Ocean Drilling Program*, 341: College Station, TX (Integrated Ocean Drilling Program). <http://dx.doi.org/10.2204/iodp.proc.341.102.2014>
- Jaeger, J.M., Gulick, S.P.S., LeVay, L.J., Asahi, H., Bahlburg, H., Belanger, C.L., Berbel, G.B.B., Childress, L.B., Cowan, E.A., Drab, L., Forwick, M., Fukumura, A., Ge, S., Gupta, S.M., Kioka, A., Konno, S., März, C.E., Matsuzaki, K.M., McClymont, E.L., Mix, A.C., Moy, C.M., Müller, J., Nakamura, A., Ojima, T., Ridgway, K.D., Rodrigues Ribeiro, F., Romero, O.E., Slagle, A.L., Stoner, J.S., St-Onge, G., Suto, I., Walczak, M.H., and Worthington, L.L., 2014b. Site U1420. In Jaeger, J.M., Gulick, S.P.S., LeVay, L.J., and the Expedition 341 Scientists, *Proceedings of the Integrated Ocean Drilling Program*, 341: College Station, TX (Integrated Ocean Drilling Program). <http://dx.doi.org/10.2204/iodp.proc.341.106.2014>
- Jaeger, J.M., Gulick, S.P.S., LeVay, L.J., Asahi, H., Bahlburg, H., Belanger, C.L., Berbel, G.B.B., Childress, L.B., Cowan, E.A., Drab, L., Forwick, M., Fukumura, A., Ge, S., Gupta, S.M., Kioka, A., Konno, S., März, C.E., Matsuzaki, K.M., McClymont, E.L., Mix, A.C., Moy, C.M., Müller, J., Nakamura, A., Ojima, T., Ridgway, K.D., Rodrigues Ribeiro, F., Romero, O.E., Slagle, A.L., Stoner, J.S., St-Onge, G., Suto, I., Walczak, M.H., and Worthington, L.L., 2014c. Site U1421. In Jaeger, J.M., Gulick, S.P.S., LeVay, L.J., and the Expedition 341 Scientists, *Proceedings of the Integrated Ocean Drilling Program*, 341: College Station, TX (Integrated Ocean Drilling Program). <http://dx.doi.org/10.2204/iodp.proc.341.107.2014>
- Koehler, R.D., Farrell, R.-E., Burns, P.A.C., and Combellick, R.A., 2012. Quaternary faults and folds in Alaska: a digital database. *Alaska Division of Geological & Geophysical Surveys Miscellaneous Publication*, 141. <http://doi.org/10.14509/23944>
- Manley, W., and Kaufman, D.S., 2002. *Alaska Paleoglacier Atlas*: Boulder, CO (Institute of Arctic and Alpine Research, University of Colorado). http://instaar.colorado.edu/QGISL/ak_paleoglacier_atlas/
- Silverman, B.W., 1985. Some aspects of the spline smoothing approach to nonparametric regression curve fitting. *Journal of the Royal Statistical Society, Series B (Methodological)*, 47(1):1–52. <http://www.jstor.org/stable/2345542>
- Walczak, M.H., Mix, A.C., Willse, T., Slagle, A., Stoner, J.S., Jaeger, J., Gulick, S., LeVay, L., Kioka, A., and the IODP Expedition 341 Scientific Party, 2015. Correction of non-intrusive drill core physical properties data for variability in recovered sediment volume. *Geophysical Journal International*, 202(2):1317–1323. <http://dx.doi.org/10.1093/gji/ggv204>
- Worthington, L.L., Gulick, S.P.S., and Pavlis, T.L., 2010. Coupled stratigraphic and structural evolution of a glaciated orogenic wedge, offshore St. Elias orogen, Alaska. *Tectonics*, 29:TC6013–TC6039. <http://dx.doi.org/10.1029/2010TC002723>
- White, R., 1997. The accuracy of well ties: practical procedures and examples. *SEG Technical Program Expanded Abstracts*, 1997(RC1):816–819. <https://doi.org/10.1190/1.1886137>
- White, R.E., 1980. Partial coherence matching of synthetic seismograms with seismic traces. *Geophysical Prospecting*, 28(3):333–358. <https://doi.org/10.1111/j.1365-2478.1980.tb01230.x>
- White, R.E., and Simm, R., 2003. Tutorial: good practice in well ties. *First Break*, 21(10):75–83.

Initial receipt: 31 August 2016

Acceptance: 15 April 2017

Publication: 28 June 2017

MS 341-204

Figure F1. Site U1419–U1421 locations (white circles). Satellite imagery (Source: esri) is draped over topography and bathymetry (Source: NGA, USGS). Red lines = major quaternary faults (Koehler et al., 2012), BT = blind thrust faults (after Worthington et al., 2010). Medium blue = maximum glacial extent during the last ~3 My, light blue = Wisconsin Last Glacial Maximum extent (Manley and Kaufman, 2002). Dashed yellow lines = approximate locations of seismic Lines GOA 2502, GOA 2503, and GOA 2505 from seismic Survey EW0408 collected aboard the R/V *Maurice Ewing* in 2004.

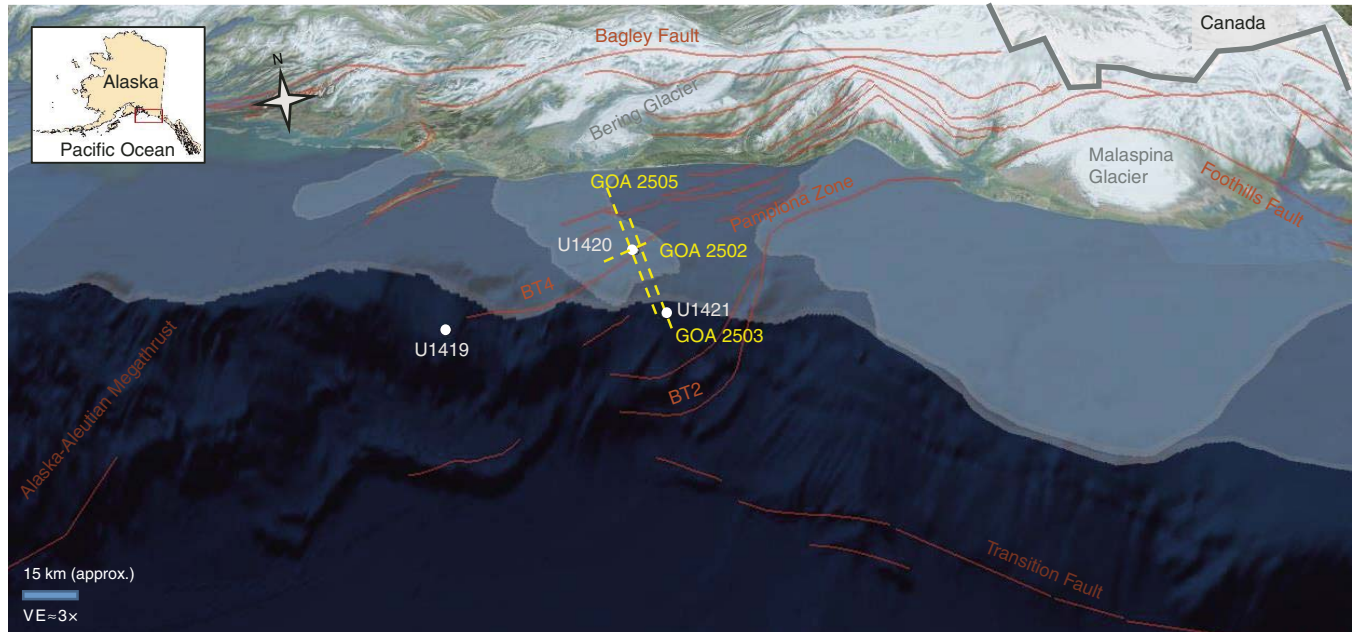


Figure F2. Schematic of general handling and relevant physical property analyses of cores collected during Expedition 341. Core handling and data collection are described in greater detail in the “Site U1420” and “Site U1421” chapters (Jaeger et al., 2014b, 2014c).

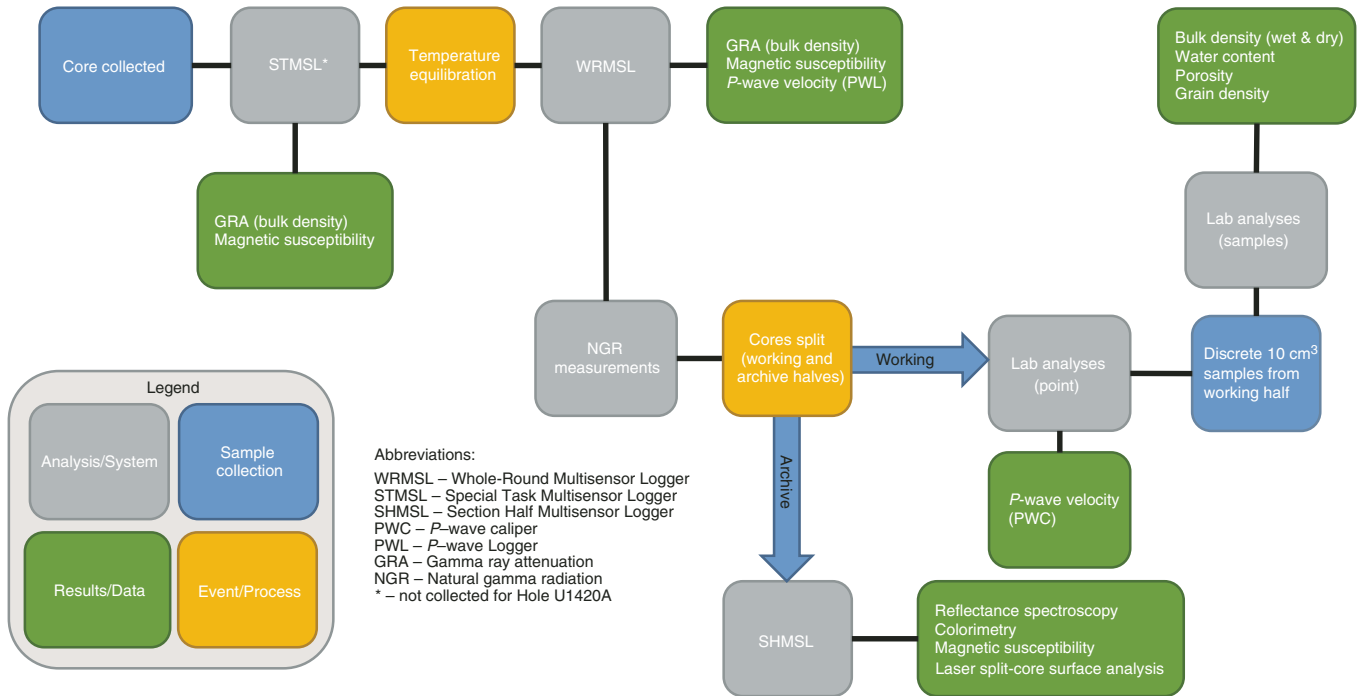


Figure F3. Summary of logs recorded by the sonic-induction tool string. Phasor dual induction–spherically focused resistivity: IDPH = deep induction, IMPH = medium induction, SFLU = shallow spherically focused resistivity. **A.** Hole U1420A. **B.** Hole U1421A. (From the [Site U1421](#) chapter [Jaeger et al., 2014c].)

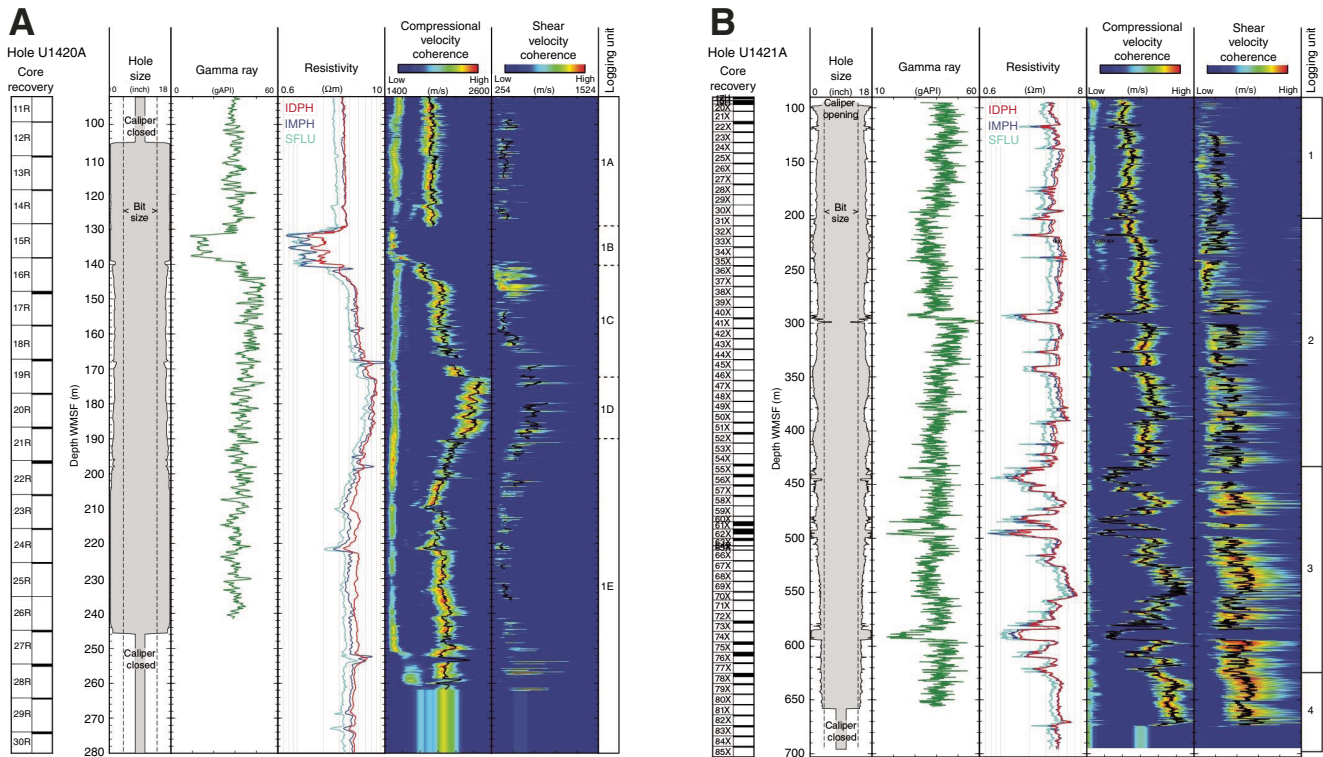


Figure F4. A. Compressional wave velocity measurements from core-compiled and log-compiled sources, Site U1421. B. Detail of interval showing overlap of core and log measurements before and after shifting the core measurements by 53 m/s to match the average of logging data. C. Compiled V_p measurements used for fitting.

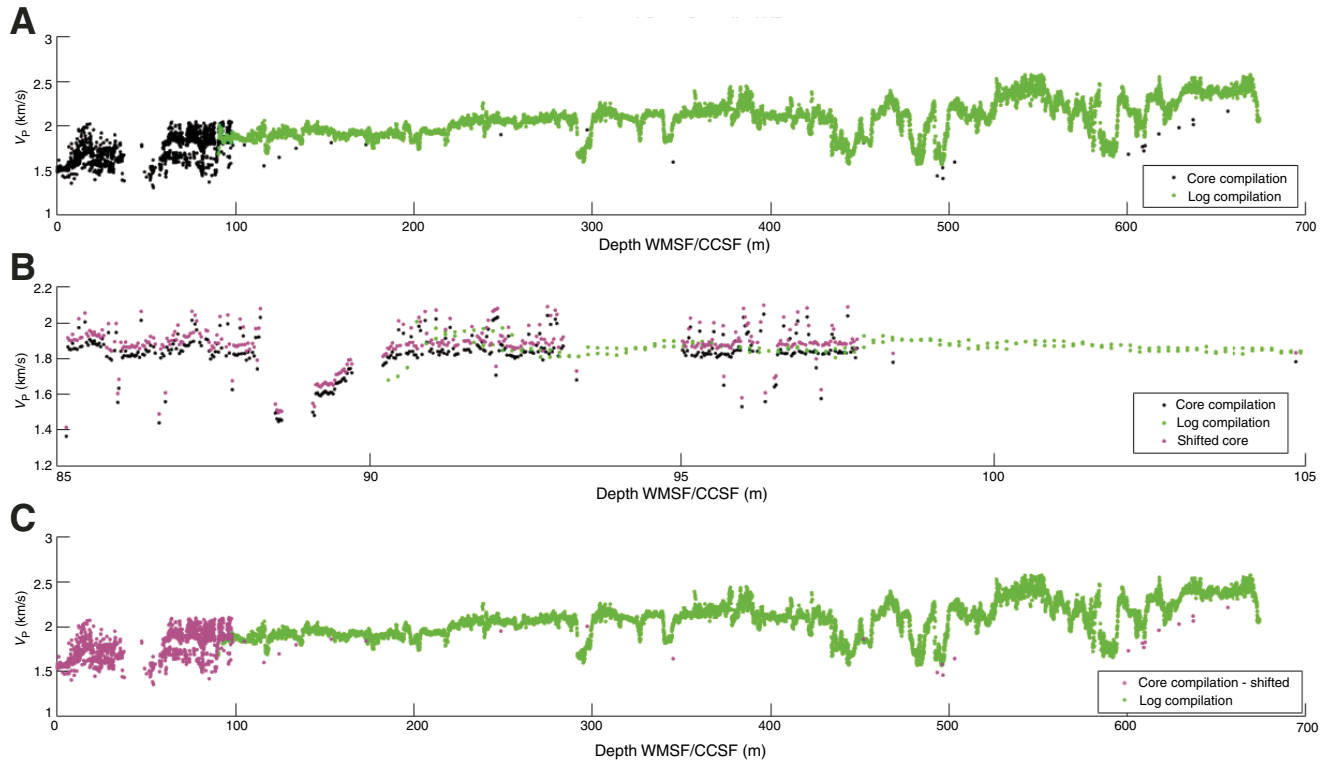


Figure F5. Bulk density compilation and fits, Site U1420. Goodness of fit characteristics for multiple spline fits derived by comparison with the moving 19-sample average. Goodness of fit characteristics are reported for respective intervals on the figure. sse = sum of squared errors, rmse = root mean squared error.

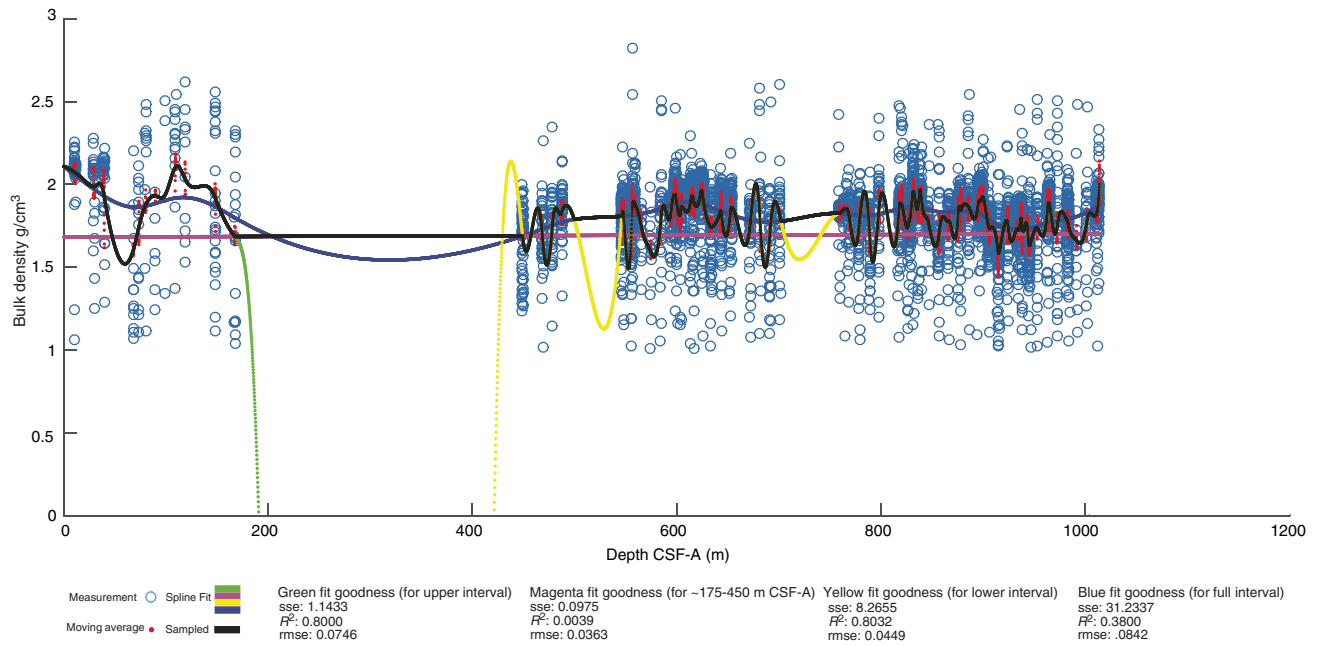


Figure F6. Compressional wave velocity measurements compilation and spline fits, Site U1420. The final sampled curve is at a rate of 0.1524 m. Goodness of fit characteristics are reported in the figure for data included in the compilation within respective intervals. In the upper interval, ~270 m, the yellow aggressively fitted curve was sampled. Deeper than 270 m on the combined depth scale, we sampled either the smoothed cyan curve for the poorly constrained intervals or the magenta curve, which we fitted aggressively for comparatively well constrained intervals. sse = sum of squared errors, rmse = root mean squared error.

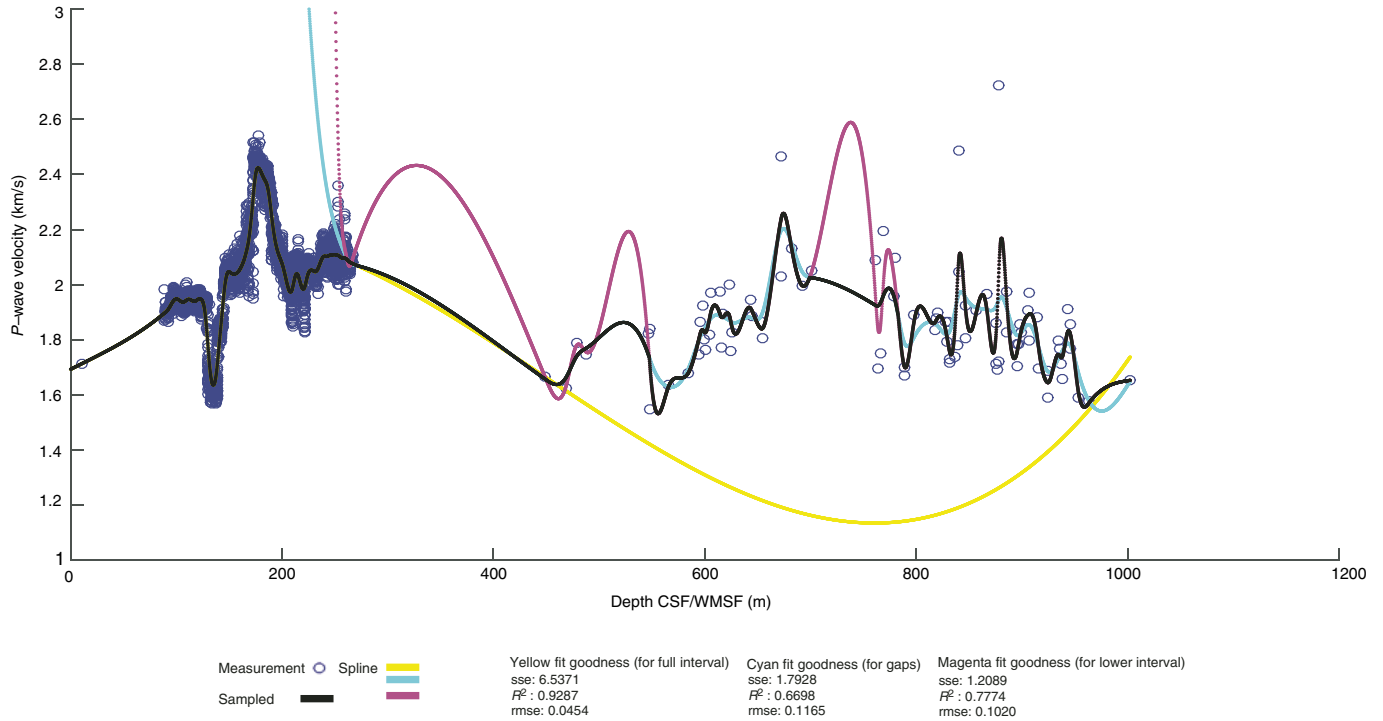


Figure F7. Bulk density compilation and fits, Site U1421. The final curve (black) was sampled at a rate of 0.1524 m. We selected the green fit for the compilation because it had the highest R^2 value such that the minimum density prediction was 1 g/cm³. For intervals near 180–220, 400–420, and 500–580 m CCSF-B, we sampled a spline fitted more conservatively for the whole data set (magenta). Measurements shown before outlier removal.

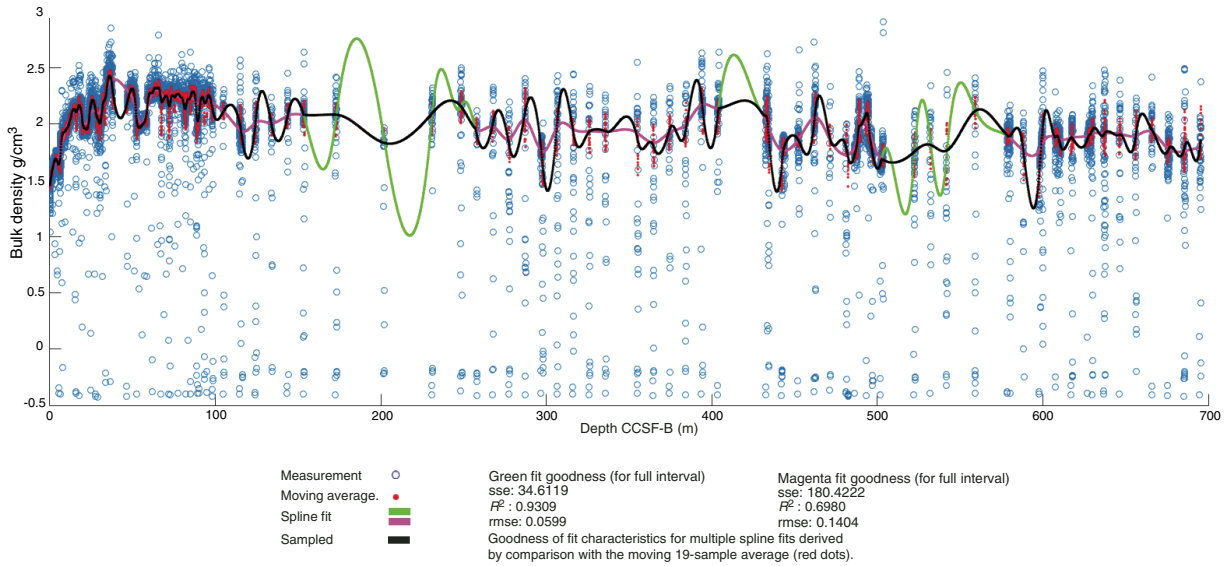


Figure F8. A. Compressional wave velocity data compilation, Site U1421. Core data and in situ logging measurements were fitted independently with two splines. B. Detail of the overlapping interval shows intersection point of the core-fitted and log-fitted splines selected to splice the curves together such that use of the logging data was prioritized. C. Final sampled curve for the full interval with core data and logging data.

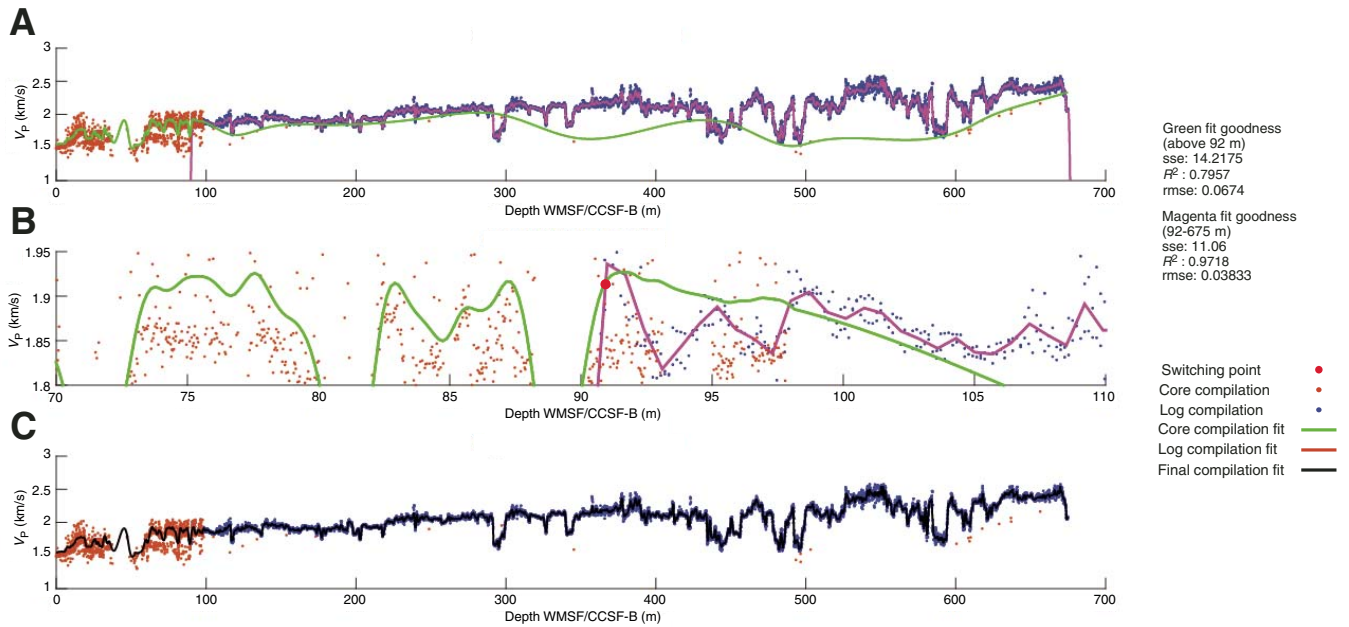


Figure F9. A. Original bulk density WRMSL data set and fit for Site U1420 shown with interpolated physical property curve sampled at 0.1524 m spacing. B. Compressional wave velocity compilation from sonic log and PWC core-derived measurements, Site U1420. Interpolated physical property curve sampled at 0.1524 m interval and fitted as described in the text. C. Original bulk density WRMSL and STMSL data set compilation and fit for Hole U1421A shown with interpolated physical property curve sampled at 0.1524 m spacing. D. Compressional wave velocity compilation from sonic log and PWC core-derived measurements, Hole U1421A. Interpolated physical property curve sampled at 0.1524 m interval and fitted as described in the text.

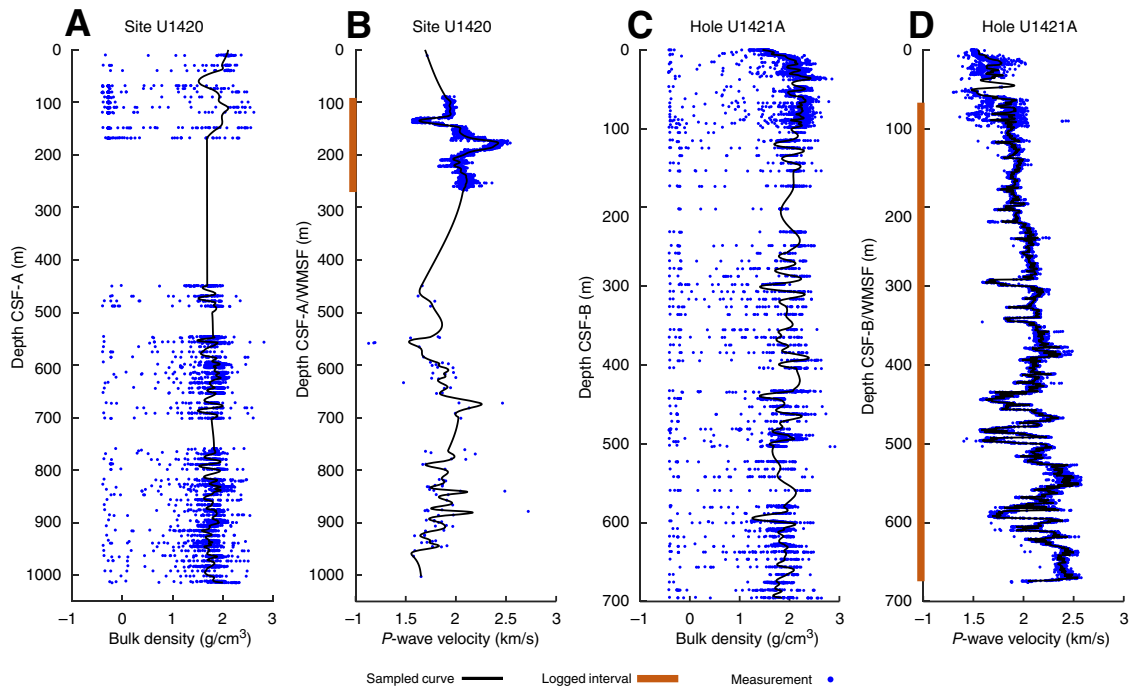


Figure F10. A. Initial interval velocity from the sonic compressional wave velocity data, Site U1420. First panel shows drift value for calibrating. Second panel shows the interval velocity from the constructed velocity curve, and third panel shows the results of calibration. The primary role of calibration in this instance is to initially match the seafloor between the velocity curve and interval velocity model and to create a 5 m sampling interval for the interval velocity. Note also that the upper interval to the seafloor is a constant velocity in the output interval velocity. TWT = two-way traveltime. B. First panel shows drift curve for sonic and VSP calibration for Site U1421. Second panel shows interval velocity from VSP check shots and seafloor constraints. Third panel shows the interval velocity for the original sonic log and the calibrated sonic log after adjusting with the drift value. The seismic depth scale below sea level (SSL) is derived from the TDR by using the logging seafloor depth and combined WMSF/CCSF/CSF scales.

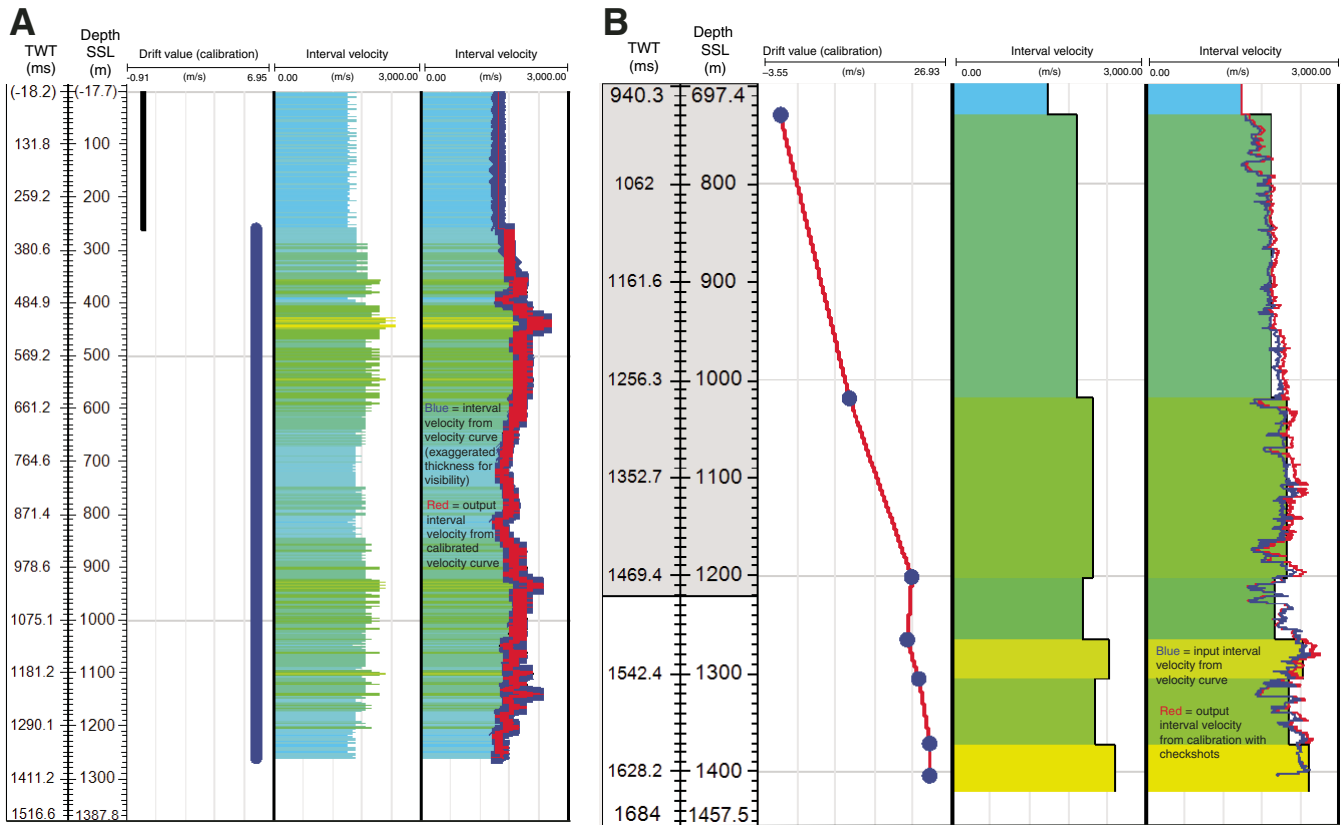


Figure F11. A. Spectral properties of initial Ricker wavelet used at each site. The Ricker wavelet was centered at 0 ms with 128 ms length. B. Spectral properties of extracted wavelet used at Site U1420 according to the Roy White method. C. Spectral properties of extracted wavelet used at Site U1421 according to the Roy White method.

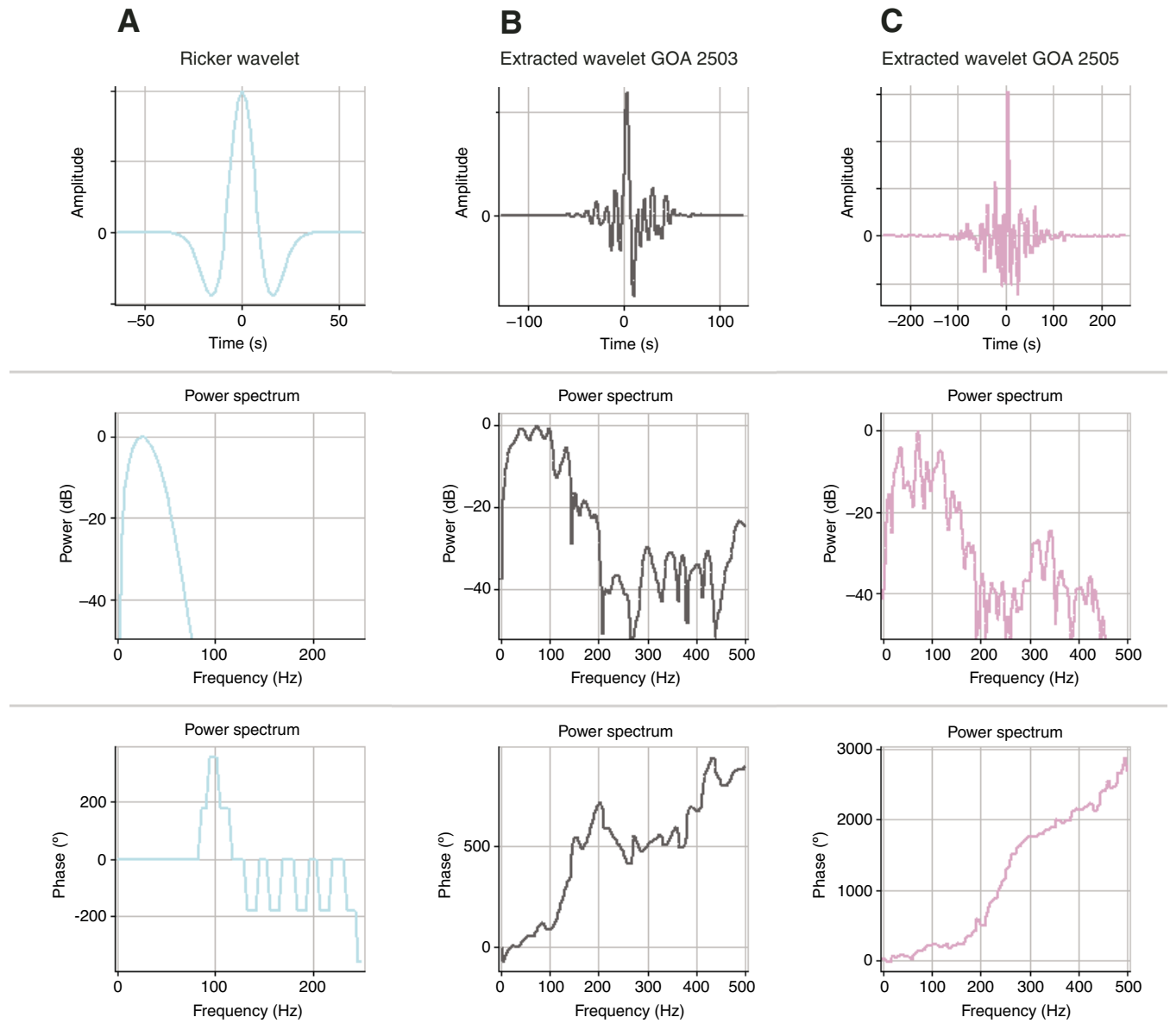


Figure F12. A. Traces from USGS 2004 EW0408 survey seismic Line GOA 2505 shown at shot locations 2617–2627 with initial TDR and visual matches (green) between the seismic and synthetic generated at Site U1420. The last two panels show the calculated interval velocity and reflectivity. Synthetic seismic was produced using the reflectivity series and the extracted wavelet shown in Figure F11C. TWT = two-way traveltime. B. Synthetic shown with seismic traces 2617–2627 and the TDR after applying the matches. The two right panels show the calculated interval velocity and reflectivity.

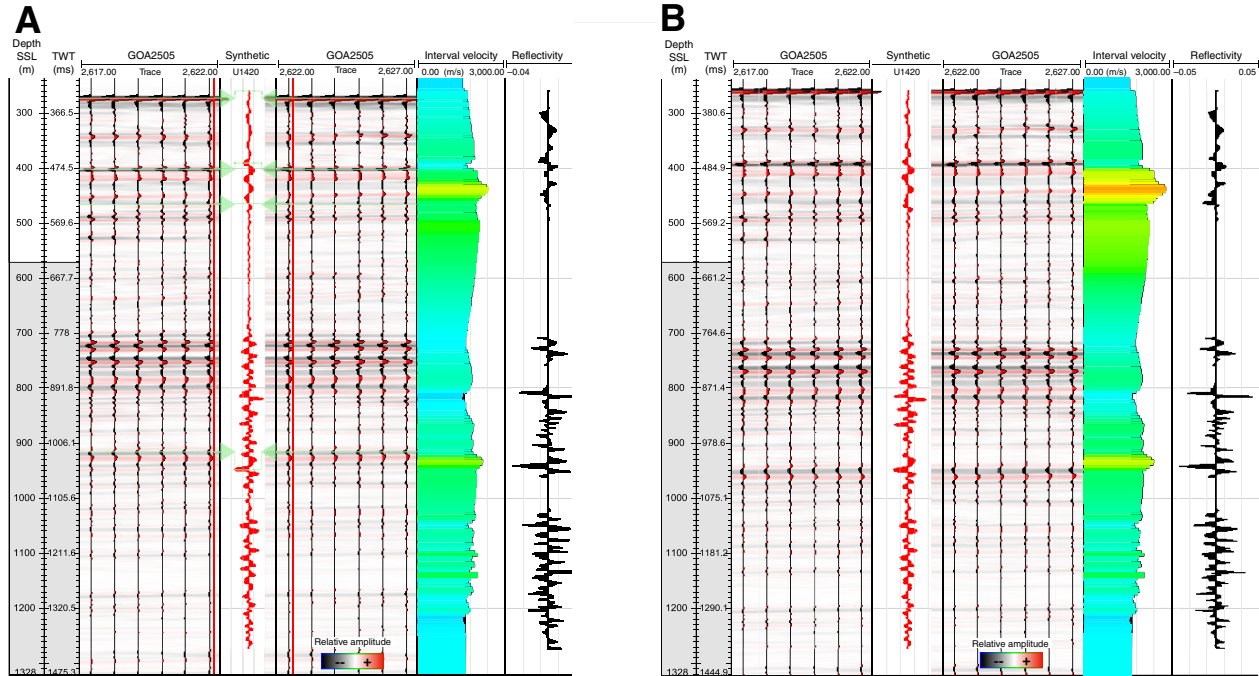


Figure F13. A. Traces from 2004 EW0408 survey seismic Line GOA 2503 shown at shot locations 406–416 with initial TDR and visual matches (green) between the seismic and synthetic. The last two panels show the calculated interval velocity and reflectivity. Synthetic seismic was produced using the reflectivity series and the extracted wavelet shown in Figure F11B. TWT = two-way traveltime. B. Synthetic shown with seismic traces 406–416 and the TDR after applying the matches. The two right panels show the calculated interval velocity and reflectivity.

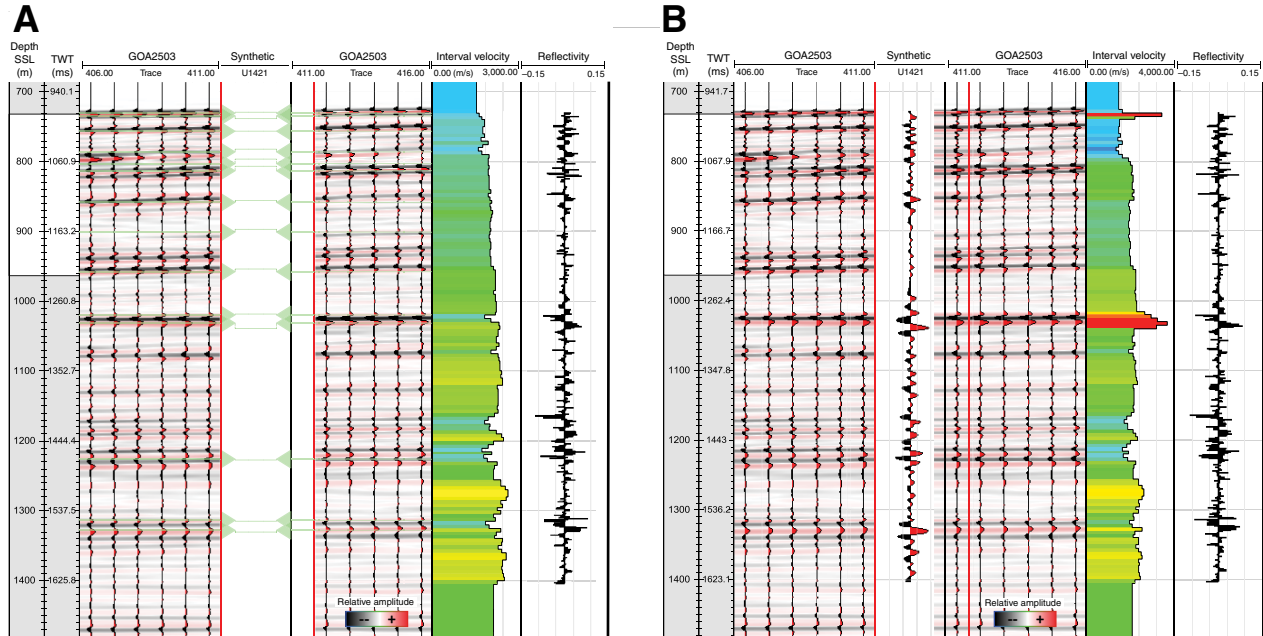


Figure F14. Cross-correlation before (left) and after (right) the tie, Site U1420. Before matching, the maximum cross-correlation within 5 traces of the site, nearest Trace 2622 on Line GOA 2505, was 0.367 with Trace 2619 with a lag of 13 ms in the 340–1410 ms window. At the site trace, the cross-correlation was calculated as -0.118 at 0 ms lag. After a bulk shift and matching, we calculate that the maximum cross-correlation occurred at Trace 2624 and 3 ms lag. At Trace 2622, the maximum cross-correlation was calculated to be 0.188 at 0 ms lag, whereas the maximum cross-correlation for this trace, 0.350, occurs with 3 ms lag. White asterisk = trace of maximum cross-correlation.

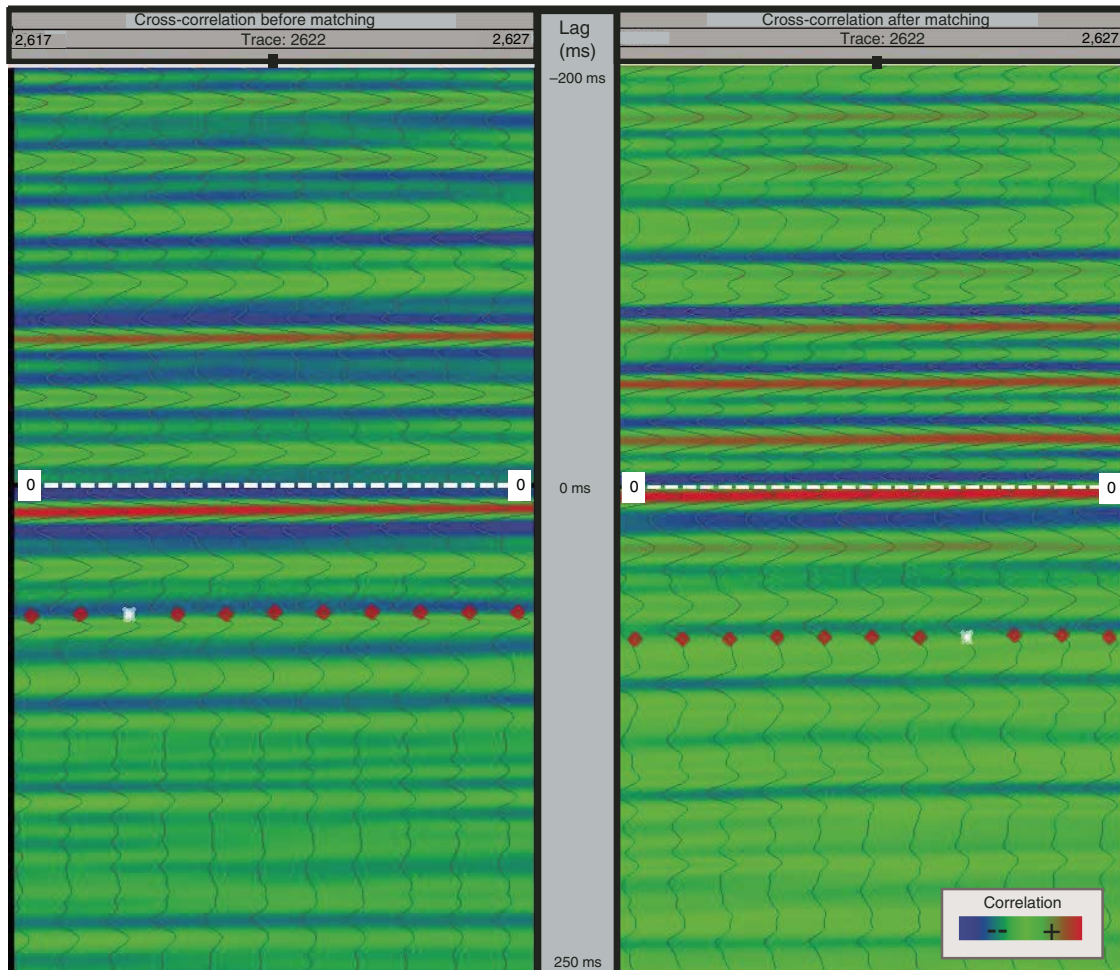


Figure F15. A. Synthetic seismic overlain for Site U1420 shown on seismic Line GOA 2505 near the site location with the final TDR. TWT = two-way traveltime. B. Synthetic seismic overlain for Site U1421 shown on Line GOA 2503 near the site location with the final TDR.

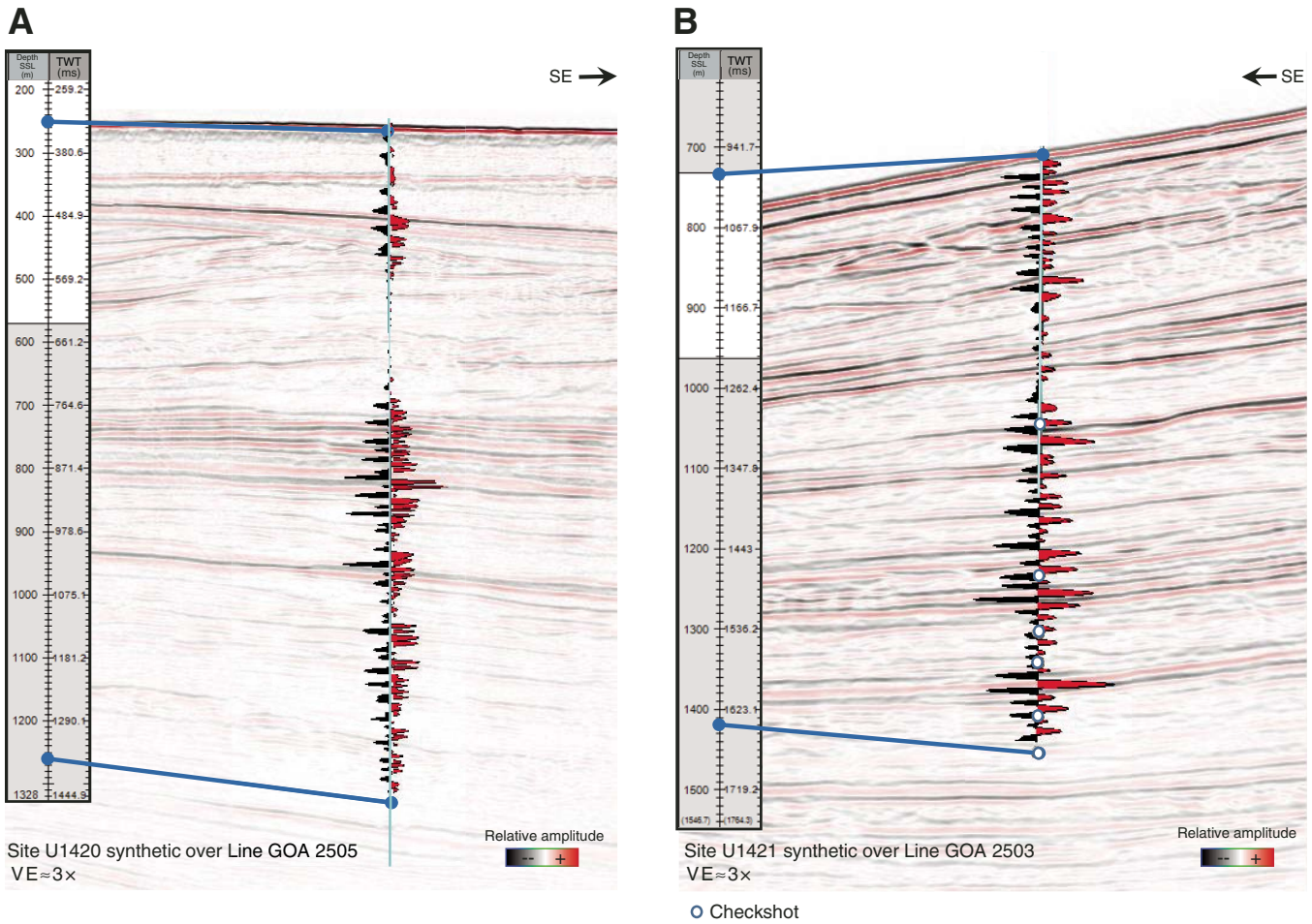


Figure F16. Cross-correlation results for the tie, Site U1421. Before matching (left), the maximum cross-correlation within 5 traces of the site, nearest Trace 411 on Line GOA 2503, was 0.417 with Trace 414 at -1 ms lag when correlating the 980–1650 ms window. At the site trace, we calculate the cross-correlation with the synthetic at 0 ms lag to be 0.365, which was also the maximum cross-correlation value in the trace window at any lag. After matching (right), the maximum cross-correlation, 0.500, occurred at Trace 413 with 0 ms lag. At Trace 411, the nearest to the site, the zero lag cross-correlation was 0.413 and the trace maximum cross-correlation, 0.448, occurred at 1 ms lag. White asterisk = trace of maximum cross-correlation.

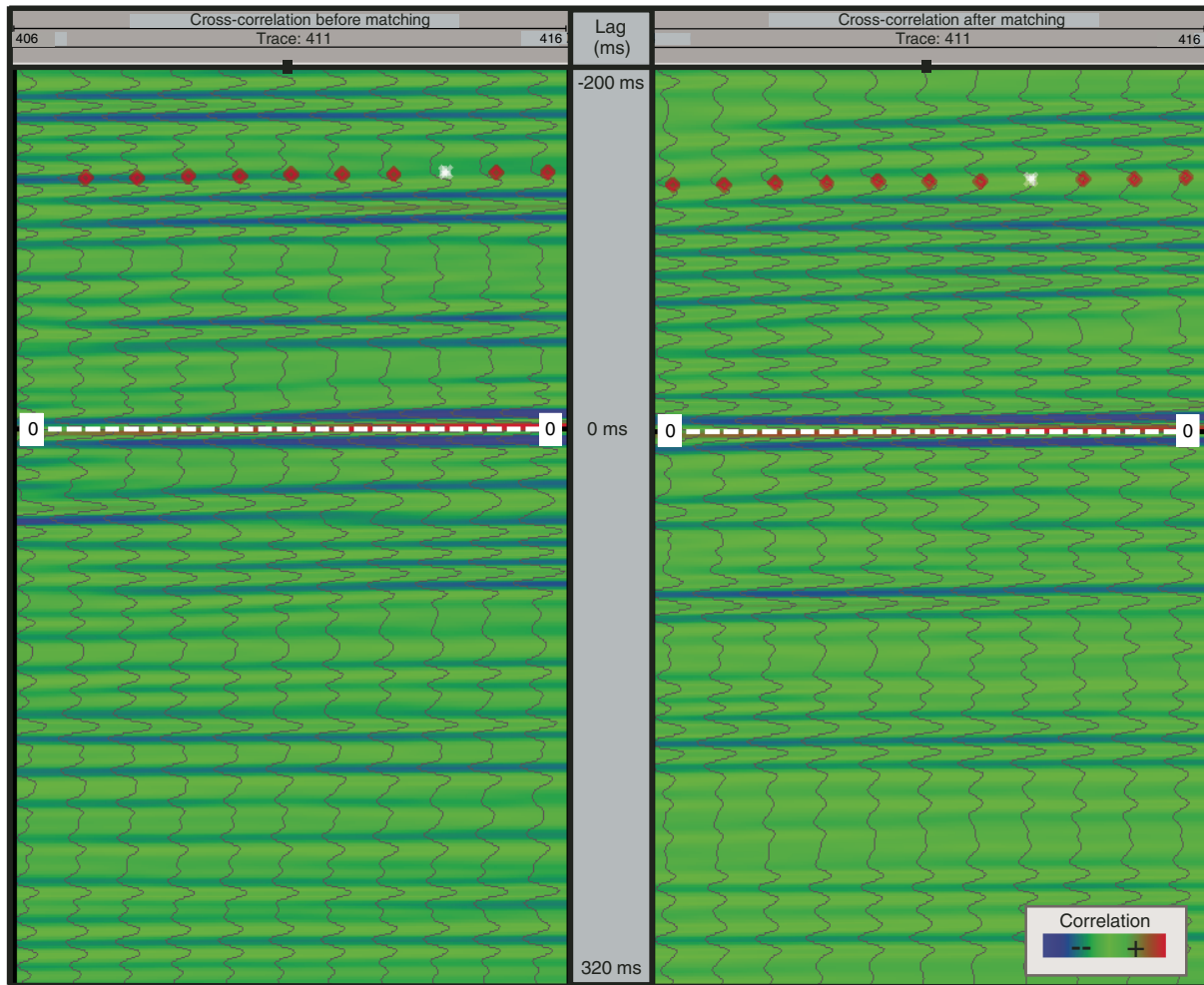


Figure F17. Horizons penetrated by drilling at (A) Site U1420 (see Fig. F30 in the Site U1420 chapter [Jaeger et al., 2014b]) and (B) Site U1421 (see Fig. F38 in the Site U1421 chapter [Jaeger et al., 2014c]) with depths interpreted using the final TDR created in this study. In each case we estimated horizon two-way traveltimes (TWTs) from seismic Lines GOA 2505 and GOA 2503, as appropriate, after the interpretations of Worthington et al. (2010) and Berger et al. (2008). Depth estimates are provided in both meters below seafloor in the seismic depth scale below seafloor (SSF) and meters seismic depth below sea level (SSL) references developed from each TDR.

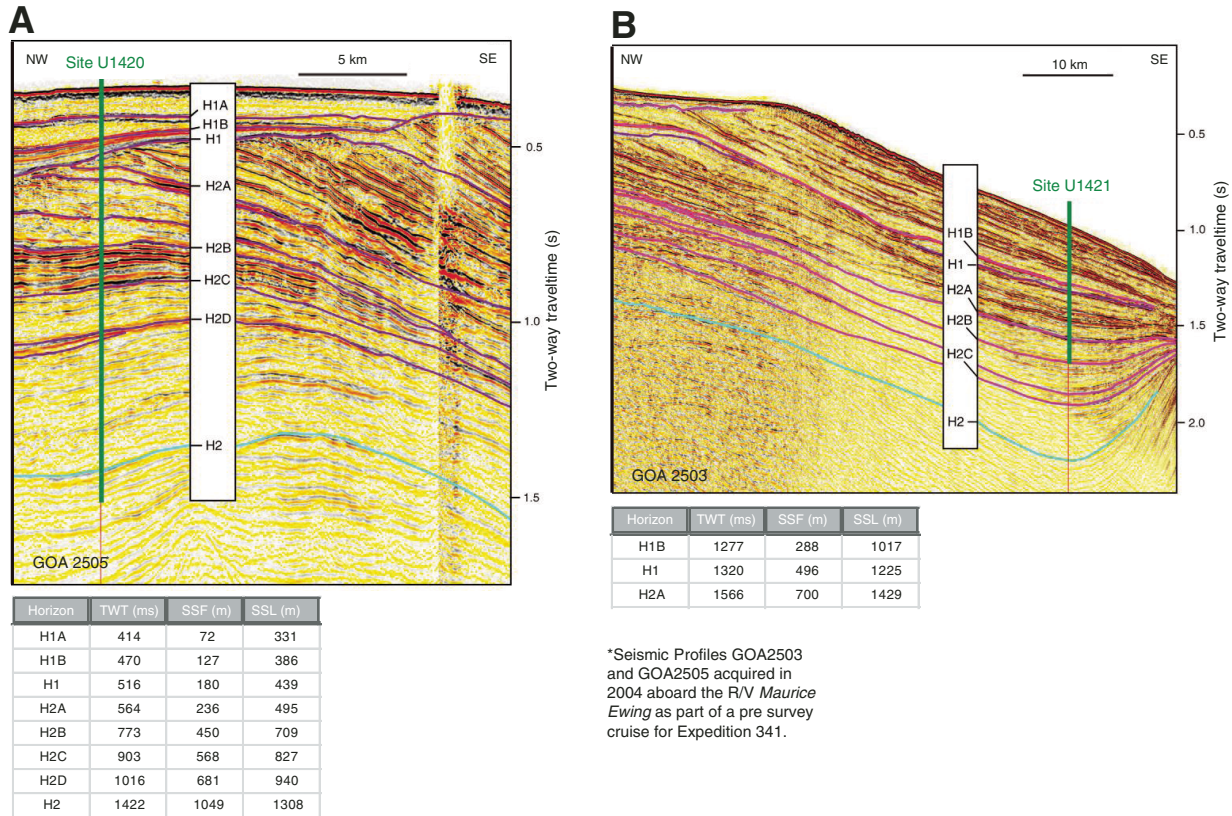


Table T1. Time-depth relationship of final tie, Site U1421.

TWT (ms)	Depth SSL (m)	Depth SSF (m)	TWT (ms)	Depth SSL (m)	Depth SSF (m)	TWT (ms)	Depth SSL (m)	Depth SSF (m)
981.5	730	1	1235.47	970	241	1453.43	1210	481
984.42	735	6	1239.95	975	246	1459.62	1215	486
988.98	740	11	1244.42	980	251	1464.78	1220	491
995.58	745	16	1248.9	985	256	1470.69	1225	496
1002.19	750	21	1253.47	990	261	1476.05	1230	501
1009.03	755	26	1257.94	995	266	1480.53	1235	506
1015.8	760	31	1262.4	1000	271	1485.2	1240	511
1022.32	765	36	1266.81	1005	276	1489.94	1245	516
1029.31	770	41	1271.2	1010	281	1494.65	1250	521
1035.44	775	46	1275.57	1015	286	1499.36	1255	526
1042.28	780	51	1279.34	1020	291	1503.62	1260	531
1049.69	785	56	1282.76	1025	296	1507.85	1265	536
1056.59	790	61	1285.86	1030	301	1511.8	1270	541
1062.7	795	66	1288.57	1035	306	1515.63	1275	546
1067.91	800	71	1291.71	1040	311	1519.44	1280	551
1072.87	805	76	1296.36	1045	316	1523.36	1285	556
1077.67	810	81	1301.02	1050	321	1527.59	1290	561
1082.5	815	86	1305.78	1055	326	1531.73	1295	566
1087.38	820	91	1310.58	1060	331	1536.17	1300	571
1092.12	825	96	1315.15	1065	336	1540.41	1305	576
1096.85	830	101	1319.9	1070	341	1545.12	1310	581
1101.65	835	106	1325.1	1075	346	1549.71	1315	586
1106.41	840	111	1329.77	1080	351	1554.85	1320	591
1111.05	845	116	1334.35	1085	356	1559.66	1325	596
1115.89	850	121	1338.84	1090	361	1563.61	1330	601
1120.55	855	126	1343.35	1095	366	1568.19	1335	606
1125.64	860	131	1347.85	1100	371	1572.94	1340	611
1130.87	865	136	1352.27	1105	376	1577.15	1345	616
1135.98	870	141	1356.74	1110	381	1581.4	1350	621
1141.01	875	146	1361.1	1115	386	1585.87	1355	626
1146.06	880	151	1365.42	1120	391	1590.11	1360	631
1151.17	885	156	1370.1	1125	396	1594.12	1365	636
1156.39	890	161	1374.74	1130	401	1598.08	1370	641
1161.59	895	166	1379.4	1135	406	1602.28	1375	646
1166.67	900	171	1384.04	1140	411	1606.46	1380	651
1171.74	905	176	1388.68	1145	416	1610.68	1385	656
1176.96	910	181	1393.3	1150	421	1614.87	1390	661
1182.03	915	186	1398.04	1155	426	1619.01	1395	666
1187.03	920	191	1402.66	1160	431	1623.08	1400	671
1192.05	925	196	1407.61	1165	436	1627.62	1405	676
1197.16	930	201	1413.05	1170	441	1632.44	1410	681
1202.28	935	206	1418.87	1175	446	1637.26	1415	686
1207.29	940	211	1424.18	1180	451	1642.09	1420	691
1212.28	945	216	1429.54	1185	456	1646.91	1425	696
1217.33	950	221	1434.29	1190	461			
1222.05	955	226	1438.72	1195	466			
1226.53	960	231	1443	1200	471			
1230.99	965	236	1447.96	1205	476			

TWT = two-way traveltime, SSL = seismic depth below sea level, SSF = seismic depth below seafloor. Bold text = data near check shots.

Table T2. Site U1420 and U1421 data summary including location and physical properties measurement availability.

Hole	Latitude	Longitude	Depth (mbrf)	Cores (N)	Interval cored (m)	Interval recovered (m)	Recovery (%)	Total penetration (m)	Total depth (mbrf)	VSP	Logged velocity (sonic)	PWC velocity	PWL velocity	Logged GRA density	STMSL bulk density	WRMSL
U1420A	59°41.3399'N	143°12.0599'W	259.4	106	1020.8	139.91	13.7	1020.8	1280.2	No	Yes	Yes	No	No	No	Yes
			Totals:	106	1020.8	139.91	13.7	1020.8								
U1421A	59°30.4399'N	143°2.7395'W	729.7	85	702.7	140.72	20.0	702.7	1432.4	Yes	Yes	Yes	Yes	No	Yes	Yes
U1421B	59°30.4284'N	143°2.7188'W	733.9	1	6.2	6.23	100.5	6.2	740.1	No	No	No	Yes	No	Yes	Yes
U1421C	59°30.4298'N	143°2.7387'W	733.0	6	38.2	29.06	76.1	38.2	771.2	No	No	No	Yes	No	Yes	Yes
			Totals:	92	747.1	176.01	23.6	747.1								

VSP = vertical seismic profile, PWC = *P*-wave caliper, PWL = *P*-wave logger, GRA = gamma ray attenuation, STMSL = Special Task Multisensor Logger, WRMSL = Whole-Round Multisensor Logger.

Table T3. Check shot data, Site U1421.

Receiver depth SSL (m)	Receiver depth SSF (m)	Corrected TWT (s)
1018.7	284.7	1.278
1201.0	467.0	1.4453
1265.0	531.0	1.50872
1304.9	570.9	1.54168
1371.0	637.0	1.60158
1421.0	687.0	1.64138

SSL = seismic depth below sea level, SSF = seismic depth below seafloor, TWT = two-way travelttime.

Table T4. Time-depth relationship, Site U1420.

TWT (ms)	Depth SSL (m)	Depth SSF (m)												
329.29	255	-4	564.72	495	236	804.2	735	476	1050.04	975	716	1307.47	1215	956
335.54	260	1	569.19	500	241	809.59	740	481	1055.02	980	721	1313.9	1220	961
341.29	265	6	573.64	505	246	814.93	745	486	1060.03	985	726	1320.26	1225	966
347.01	270	11	578.1	510	251	820.23	750	491	1065.04	990	731	1326.53	1230	971
352.68	275	16	582.55	515	256	825.48	755	496	1070.08	995	736	1332.74	1235	976
358.33	280	21	587.03	520	261	830.69	760	501	1075.15	1000	741	1338.88	1240	981
363.97	285	26	591.52	525	266	835.84	765	506	1080.24	1005	746	1345	1245	986
369.55	290	31	596.06	530	271	840.95	770	511	1085.35	1010	751	1351.09	1250	991
375.11	295	36	600.59	535	276	846.02	775	516	1090.5	1015	756	1357.17	1255	996
380.63	300	41	605.14	540	281	851.06	780	521	1095.67	1020	761	1363.22	1260	1001
386.13	305	46	609.71	545	286	856.1	785	526	1100.86	1025	766	1369.24	1265	1006
391.59	310	51	614.29	550	291	861.14	790	531	1105.99	1030	771	1375.24	1270	1011
397.01	315	56	618.88	555	296	866.23	795	536	1111.02	1035	776	1381.24	1275	1016
402.4	320	61	623.5	560	301	871.39	800	541	1116.13	1040	781	1387.24	1280	1021
407.75	325	66	628.13	565	306	876.68	805	546	1121.52	1045	786	1393.24	1285	1026
413.07	330	71	632.78	570	311	882.28	810	551	1127.35	1050	791	1399.24	1290	1031
418.35	335	76	637.46	575	316	888.33	815	556	1133.05	1055	796	1405.24	1295	1036
423.58	340	81	642.15	580	321	894.4	820	561	1138.39	1060	801	1411.24	1300	1041
428.79	345	86	646.88	585	326	900.23	825	566	1143.6	1065	806	1417.24	1305	1046
433.94	350	91	651.62	590	331	905.92	830	571	1148.87	1070	811	1423.24	1310	1051
439.03	355	96	656.4	595	336	911.57	835	576	1154.21	1075	816	1429.24	1315	1056
444.06	360	101	661.2	600	341	917.21	840	581	1159.58	1080	821	1435.24	1320	1061
449.09	365	106	666.03	605	346	922.81	845	586	1164.89	1085	826	1441.24	1325	1066
454.13	370	111	670.89	610	351	928.26	850	591	1170.4	1090	831	1447.24	1330	1071
459.16	375	116	675.78	615	356	933.5	855	596	1176.06	1095	836	1453.24	1335	1076
464.19	380	121	680.7	620	361	938.63	860	601	1181.15	1100	841	1459.24	1340	1081
469.21	385	126	685.66	625	366	943.66	865	606	1186.03	1105	846	1465.24	1345	1086
474.54	390	131	690.65	630	371	948.54	870	611	1191.4	1110	851	1471.24	1350	1091
479.93	395	136	695.67	635	376	953.48	875	616	1196.81	1115	856	1477.24	1355	1096
484.94	400	141	700.74	640	381	958.44	880	621	1202	1120	861	1483.24	1360	1101
489.43	405	146	705.83	645	386	963.44	885	626	1207.1	1125	866	1489.24	1365	1106
493.64	410	151	710.98	650	391	968.59	890	631	1212.51	1130	871	1495.24	1370	1111
497.83	415	156	716.15	655	396	973.66	895	636	1218.14	1135	876	1501.24	1375	1116
502.01	420	161	721.36	660	401	978.59	900	641	1223.02	1140	881	1507.24	1380	1121
506.11	425	166	726.62	665	406	983.51	905	646	1227.89	1145	886	1513.24	1385	1126
510.06	430	171	731.93	670	411	988.53	910	651	1233.4	1150	891	1519.24	1390	1131
513.71	435	176	737.27	675	416	993.62	915	656	1239.15	1155	896	1525.24	1395	1136
517.26	440	181	742.65	680	421	998.58	920	661	1244.65	1160	901	1531.24	1400	1141
520.86	445	186	748.08	685	426	1003.24	925	666	1249.98	1165	906	1537.24	1405	1146
524.59	450	191	753.56	690	431	1007.58	930	671	1255.27	1170	911	1543.24	1410	1151
528.56	455	196	759.08	695	436	1011.76	935	676	1260.75	1175	916	1549.24	1415	1156
532.65	460	201	764.64	700	441	1016.01	940	681	1266.6	1180	921	1555.24	1420	1161
536.88	465	206	770.26	705	446	1020.48	945	686	1272.66	1185	926			
541.62	470	211	775.91	710	451	1025.22	950	691	1278.61	1190	931			
546.24	475	216	781.62	715	456	1030.23	955	696	1284.37	1195	936			
550.93	480	221	787.34	720	461	1035.2	960	701	1290.08	1200	941			
555.58	485	226	793.05	725	466	1040.14	965	706	1295.57	1205	946			
560.15	490	231	798.7	730	471	1045.09	970	711	1301.28	1210	951			

Time-depth relationship is interpolated for deeper than ~1260 m seismic depth below sea level (SSL). SSF = seismic depth below seafloor.